MCB
Journals.ASM.org

Berardinelli-Seip Congenital Lipodystrophy 2/Seipin Is a Cell-Autonomous Regulator of Lipolysis Essential for Adipocyte Differentiation

Weiqin Chen,[a] Benny Chang,[a,b] Pradip Saha,[a] Sean M. Hartig,[b] Lan Li,[a] Vasumathi Theegala Reddy,[a] Yisheng Yang,[a] Vijay Yechoor,[a] Michael A. Mancini,[b] and Lawrence Chan[a,b,c,d]

Diabetes and Endocrinology Research Center, Division of Diabetes, Endocrinology and Metabolism, Departments of Medicine,[a] Molecular & Cellular Biology,[b] and Biochemistry,[c] Baylor College of Medicine, and St. Luke's Episcopal Hospital,[d] Houston, Texas, USA

Mutations in BSCL2 underlie human congenital generalized lipodystrophy. We inactivated Bscl2 in mice to examine the mechanisms whereby absence of Bscl2 leads to adipose tissue loss and metabolic disorders. *Bscl2*$^{-/-}$ mice develop severe lipodystrophy of white adipose tissue (WAT), dyslipidemia, insulin resistance, and hepatic steatosis. *In vitro* differentiation of both *Bscl2*$^{-/-}$ murine embryonic fibroblasts (MEFs) and stromal vascular cells (SVCs) reveals normal early-phase adipocyte differentiation but a striking failure in terminal differentiation due to unbridled cyclic AMP (cAMP)-dependent protein kinase A (PKA)-activated lipolysis, which leads to loss of lipid droplets and silencing of the expression of adipose tissue-specific transcription factors. Importantly, such defects in differentiation can be largely rescued by inhibitors of lipolysis but not by a gamma peroxisome proliferator-activated receptor (PPARγ) agonist. The residual epididymal WAT (EWAT) in *Bscl2*$^{-/-}$ mice displays enhanced lipolysis. It also assumes a "brown-like" phenotype with marked upregulation of UCP1 and other brown adipose tissue-specific markers. Together with decreased Pref1 but increased C/EBPβ levels, these changes highlight a possible increase in cAMP signaling that impairs terminal adipocyte differentiation in the EWAT of *Bscl2*$^{-/-}$ mice. Our study underscores the fundamental role of regulated cAMP/PKA-mediated lipolysis in adipose differentiation and identifies Bscl2 as a novel cell-autonomous determinant of activated lipolysis essential for terminal adipocyte differentiation.

Obesity and lipodystrophy are opposites in terms of an excess versus deficiency of total body fat, and yet these conditions display overlapping metabolic consequences, including insulin resistance, dyslipidemia, hepatic steatosis, and increased risk for diabetes as well as cardiovascular diseases (CVD) (38). Congenital generalized lipodystrophy (CGL; also called Berardinelli-Seip congenital lipodystrophy [BSCL]) is an autosomal recessive disorder characterized by a near total absence of body fat from birth or infancy (4, 37). Mutations in the *BSCL2* gene (also called seipin) cause type 2 CGL (CGL2), the most severe form of CGL (26). BSCL2 is highly conserved among species from *Caenorhabditis elegans* to *Homo sapiens* (26). The protein resides in the endoplasmic reticulum (ER) (11, 33, 42) and is expressed in most tissues, with the highest level in the testes and neuronal and adipose tissue (2, 11, 26).

Most of the *BSCL2* mutations in CGL patients involve nonsense, splice, or frameshift mutations, which likely result in complete loss of function (26). In both yeast and human fibroblasts, Bscl2 is required for normal lipid droplet (LD) assembly and maintenance (6, 15, 41). Knockdown experiments in mouse adipogenic cell lines have suggested that Bscl2 plays a direct role in adipocyte differentiation through an as-yet-unknown mechanism (11, 33).

Adipocyte differentiation is accompanied by increased triglyceride synthesis with low-level lipolysis. Lipolysis is tightly regulated via adipocyte triglyceride lipase (ATGL) (17) and modulation of intracellular concentrations of cyclic AMP (cAMP). cAMP-activated PKA-mediated phosphorylation of Perilipin 1 (Plin1) and hormone-sensitive lipase (HSL) is a critical event for the activation and recruitment of HSL to lipid droplets (31), where it acts in concert with ATGL to hydrolyze stored lipids (48). Maintaining the delicate balance between triglyceride synthesis and lipolysis is essential for normal adipose tissue function, whereas an imbalance of these processes can result in lipodystrophy or obesity.

To address the molecular basis of adipose tissue deficiency in the absence of Bscl2, we created Bscl2-deficient mice by gene targeting. We found that *Bscl2*$^{-/-}$ mice recapitulated most of the lipodystrophic presentations of human CGL2. While we were preparing our manuscript for publication, Cui et al. reported the creation of *Bscl2*$^{-/-}$ mice and found that these mice had lost most of their body fat (13); however, those authors did not explore the mechanisms that underlie the observation. Extensive *in vivo* and *in vitro* analysis of our mice revealed that properly controlled lipolysis is essential for normal adipogenesis and uncovered for the first time that Bscl2 is an upstream negative regulator of activated lipolysis and a cell-autonomous determinant of adipocyte differentiation whose deletion produces unbridled lipolysis that leads to aborted adipogenesis and lipodystrophy.

Received 24 October 2011 **Returned for modification** 23 November 2011
Accepted 12 January 2012
Published ahead of print 23 January 2012
Address correspondence to Lawrence Chan, lchan@bcm.edu.
Supplemental material for this article may be found at http://mcb.asm.org/.

doi:10.1128/MCB.06465-11

MATERIALS AND METHODS

Generation of Bscl2-deficient mice. Details of targeting vector construction, embryonic stem (ES) cell culture, *Bscl2*-deficient mouse generation, and genotyping were described in the supplemental material. Mice were maintained under standard conditions with controlled light and temperature and fed with a chow diet *ad libitum*. All animal experiments were done using protocols approved by the IACUC at Baylor College of Medicine.

Blood and plasma biochemistry. Blood glucose tests were performed with a OneTouch UltraSmart blood glucose monitoring system (Life Scan). Plasma nonesterified fatty acid (NEFA) (Wako), glycerol (Sigma), total cholesterol, and total triacylglycerol (TAG; Therma DMA) levels were measured colorimetrically. Serum insulin (Mercodia), leptin (R&D Diagnostics), and adiponectin (R&D Diagnostics) levels were measured by enzyme-linked immunosorbent assays according to the instructions of the manufacturers.

Magnetic resonance spectroscopy (MRS) and whole-body fat content measurement. *In vitro* whole-body mouse imaging was performed utilizing a Bruker Biospec AVANCE 9.4T spectrometer (Bruker Biospin) (72-mm resonator). Two mice were imaged together by placing them into two 50-ml conical tubes (Franklin Lakes, NJ) bundled together. A T1-weighted three-dimensional (3D) spin-echo sequence was used for best fat contrast with the following parameters: repetition time, 400.0 ms; echo time, 10.3 ms; field of view (FOV), 55 by 90 by 30 mm; matrix size, 256 by 512 by 256 pixels; slice thickness, 1.0 mm; scan time, 14 h 34 min. The 3D images were reconstructed using Amira software after careful removal of signals from mouth and stomach due to ingested food in both genotypes. Whole-body fat content was measured by using an EchoMRI whole-body composition analyzer (Echo Medical Systems) according to the manufacturer's instructions.

Food intake measurement. Food intake was measured in 13-week-old male wild-type (WT) and *Bscl2*$^{-/-}$ mice (9 mice per group) by the use of a comprehensive laboratory animal monitoring system (CLAMS; open-circuit oxygen consumption Oxymax system, version 2.1.0) (Columbus Instruments, Columbus, OH). Data were normalized to body weights.

Isolation and differentiation of MEFs and stromal vascular cells (SVCs). mouse embryonic fibroblasts (MEFs) were isolated from 12.5- to 14.5-day-old embryos and cultured in high-glucose Dulbecco's modified Eagle's medium (DMEM) supplemented with 10% fetal bovine serum (FBS; Invitrogen) and penicillin-streptomycin (Pen/Strep). Subcutaneous adipose tissues from 6-week-old wild-type and *Bscl2*$^{-/-}$ mice were digested with collagenase type IV at 37°C for 40 to 60 min, and the digest was filtered through a 100-μm-pore-size mesh. The stromal vascular fraction containing the preadipocytes was centrifuged at 800 $\times$ *g* for 10 min, and the cells were resuspended and cultured in high-glucose FBSDMEM containing 10% fetal bovine serum and Pen/Strep.

MEF or SVC cells were plated at same density and meticulously maintained until 2 days after confluence (day 0). Differentiation was induced by culturing cells in commercial adipocyte differentiation medium (ADM; Cell Applications) for 2 days followed by regular media (high-glucose DMEM plus 10% FBS and Pen/Strep) in the presence of 100 μM insulin alone for another 2 days. Cells were then kept on regular medium, and the medium was changed every 2 days. Differentiated cells were either visualized using light microscopy or stained using Oil-Red O staining. Medium samples were generally taken at 2-day intervals when changing media to follow glycerol (Sigma) concentrations as an index for lipolysis. In some experiments, the lipase inhibitor diethyl-*p*-nitrophenylphosphate (E600; Sigma) (200 μM) (9), H89 (a potent protein kinase A [PKA] inhibitor) (10 μM) (45), forskolin (10 μM), and 3-isobutyl-1-methylxanthine (IBMX) (0.5 mM) were added at day 4 (pioglitazone [1 μM] was added at day 0) and constantly maintained in the later culture, with vehicle included in the control cells. Other than much lower initial differentiation efficiency in comparison with ADM, we observed similar results by using conventional differentiation cocktails (dexamethasone, IBMX, and insulin) in the first 2 days to induce differentiation.

Tissue and intracellular TAG analyses, Oil-Red O staining, and measurement of TAG synthesis. Tissues were homogenized in standard phosphate-buffered saline (PBS) buffer. Lipids were extracted according to the method of Bligh and Dyer (5) and dissolved in 5% Triton X-100–PBS. Cultured cells were directly lysed in 1% Triton X-100–PBS. Triglyceride concentrations were measured using a triglyceride assay kit (Thermo DMA) and normalized to tissue weights or protein concentrations (cell). Oil-Red O staining was performed as described previously (19), and the results were photographed with a camera with or without microscopy. Measurement of TAG synthesis in day 4 differentiating MEF cells is detailed in the supplemental material.

Histology and immunofluorescence microscopy. Tissues were fixed with neutral-buffered formalin and embedded in paraffin. Sections (7 μM) were stained with hematoxylin-eosin. Images were analyzed using a Zeiss Axioplan-2 imaging system.

MEF cells were plated on collagen-coated glass coverslips. At the indicated days of differentiation, cells were fixed with 4% paraformaldehyde, permeabilized with 0.2% NP-40, blocked with 5% goat serum, and then probed with specific primary antibodies and subsequently labeled with fluorescence-tagged secondary antibodies as well as with LipidTOX (Invitrogen) for staining of neutral lipids. Coverslips were then mounted with SlowFade Gold mounting media (Invitrogen). Images were taken with a DeltaVision (Deconvolution) image restoration microscope or a Zeiss Axioplan-2 imaging system.

Reverse transcription, real-time PCR, and nuclear DNA content analyses. Total RNA was isolated from tissues or cultured cells with TRIzol (Invitrogen) and subjected to reverse transcription (RT) using Superscript II reverse transcriptase and random primers (Invitrogen). Real-time quantitative RT-PCR (qPCR) was performed using a Stratagene Mx3000 system. Relative amounts of nuclear DNA were determined by quantitative real-time PCR using primers for intron 9 of the nucleus-specific hexokinase 2 gene as described previously (21).

Lipolysis performed *in vitro*, *in vivo*, and *ex vivo*. Lipolysis was performed *in vitro* on day 4 differentiating MEF cells. Briefly, after the cells were washed twice with phosphate-buffered saline (PBS), cells were incubated in 2% bovine serum albumin (BSA) medium in the presence or absence of 10 μM ß3 adrenergic receptor agonist CL 316243. Media were collected at 2 h for glycerol and NEFA level determinations. For *in vivo* lipolysis, mice were fasted for 4 h and treated with an intraperitoneal injection of CL 316243 (0.1 mg per kg of body weight). Blood was collected before and 15 min after injection for determination of NEFA and glycerol levels. Data were also normalized to total fat mass contents based on EchoMRI. For *ex vivo* lipolysis, epididymal fat was removed postmortem and cut into 10- to 15-mg fat pads. Fat pads were distributed into 48-well plates containing 0.25 ml DMEM–2% free fatty acid (FFA)-free BSA media in the presence or absence of CL 316243 (Sigma-Aldrich) (10 μM) for 2 h at 37°C in a humidified atmosphere (95% O_2, 5% CO_2), with an explant from each animal (n = 5/genotype/experiment) being allocated to each *in vitro* treatment group. The medium was then collected for determination of glycerol levels. The tissue was weighed on a torsion balance, and the data were expressed per milligram of wet weight.

Lipid droplet fractionation from cells and tissues. Day 4 MEF adipocytes were harvested from three 10-cm plates and homogenized in 2.0 ml of cold 250-STMDPS (250 mM sucrose, 50 mM Tris-HCl, 5 mM $MgCl_2$, 1 mM dithiothreitol [DTT], spermidine [25 μg/ml], protease inhibitor cocktail [Sigma]) buffer in a Teflon glass homogenizer with 12 gentle strokes. Epididymal white adipose tissues (EWAT) were disrupted in a nitrogen bomb (Parr Instrument). LD fractions were isolated as described by Liu et al. (24). Briefly, total homogenate was centrifuged at 10,000 $\times$ *g* for 10 min to remove debris. The supernatant was mixed well and subjected to further ultracentrifugation at 45,000 $\times$ *g* for 1 h to separate and recover the floating LD fraction. Proteins associated with lipid

droplets were solubilized by incubation for 2 h at 37°C in a sonicating water bath.

Immunoblot analysis. Total cell lysates were prepared with a lysis buffer containing 25 mM Tris-HCl (pH 7.4), 150 mM NaCl, 2 mM EDTA, 1% Triton X-100, and 10% glycerol with freshly added protease inhibitor cocktail (Sigma) plus 50 mM NaF, 10 mM sodium pyrophosphate, and 1 mM sodium vanadate. Identical amounts of proteins were loaded, and immunoblot analysis was carried out according to the standard protocol. The following antibodies were used: PLIN1 (Progen Biotechnik GmbH); p-Perilipin-Ser 522 (mouse 517) (kind gift of Patrick M. McDonough, Vala Sciences); ATGL (Caymen Chemicals); HSL and phospho-HSL (Ser563) antibodies (Cell Signaling Technology); ap2 (R&D Systems); gamma peroxisome proliferator-activated receptor (PPARγ) (Cell Signaling); GAPDH (glyceraldehyde-3-phosphate dehydrogenase; Fisher Scientific); and β-actin (Chemicon). Image J was used to quantify the intensity of the bands.

Measurement of cAMP concentrations. Intracellular cAMP concentrations were measured by immunoassay following the instructions of the manufacturer (R&D Systems). cAMP content was normalized to total protein and expressed as picomoles per milligram of protein.

Cellular metabolic rate. We washed day 4 MEF differentiating adipocytes with 1 ml of XF-DMEM (catalog no. D5030; Sigma-Aldrich) containing sodium pyruvate (1 mmol/liter), GlutaMAX-1 (2 mmol/liter), glucose (17.5 mmol/liter), NaCl (1.85 g/liter), and phenol red (pH 7.4) (15 mg/liter) and added 500 μl per well. The oxygen consumption rate (OCR [aerobic respiration]) and extracellular acidification rate (ECAR [anaerobic respiration]) were measured (model XF24 extracellular flux analyzer; Seahorse Bioscience) as described previously (43, 47).

Statistical analysis. Quantitative data are presented as means ± standard errors of the means (SEM). Representative results from at least three independent experiments are shown for *in vitro* experiments performed with MEFs. Differences between groups were examined for statistical significance with a 2-tailed Student's *t* test. A *P* value of less than 0.05 was considered statistically significant.

RESULTS

Bscl2-deficient mice have severe congenital generalized lipodystrophy and hepatic steatosis. We generated Bscl2-deficient mice as described for Fig. S1A and S1B in the supplemental material. Bscl2 transcripts were essentially absent in epididymal white adipose tissue (EWAT) and subcutaneous white adipose tissue (ScWAT) and brown adipose tissue (BAT) of *Bscl2*$^{-/-}$ mice (see Fig. S1C in the supplemental material). The transcript levels of Gng3, a divergently transcribed gene adjacent to Bscl2, were not significantly different in the EWAT, ScWAT, and BAT of *Bscl2*$^{+/+}$ and *Bscl2*$^{-/-}$ mice, indicating that specific deletion of *Bscl2* does not affect the expression of this neighboring gene (see Fig. S1D in the supplemental material). *Bscl2*$^{-/-}$ mice were born from *Bscl2*$^{+/-}$ parents with the expected Mendelian distribution. During the neonatal period, however, *Bscl2*$^{-/-}$ mice displayed an increased early postnatal mortality rate (21% compared with 11% in wild-type and 9% in heterozygous mice by 3 weeks). They were smaller during the first 3 weeks of life but caught up in size with wild-type littermates at week 4 after weaning (see Fig. S1E in the supplemental material). Whole-body magnetic resonance spectroscopy revealed generalized loss of subcutaneous, interscapular, perirenal, and gonadal WAT in 12-week-old male (Fig. 1A) and female (data not shown) *Bscl2*$^{-/-}$ mice. EchoMRI quantification indicated a 72% reduction of total body fat mass and a 3.5% increase in lean mass in *Bscl2*$^{-/-}$ mice compared with their wild-type counterparts (Fig. 1B). On dissection, *Bscl2*$^{-/-}$ mice displayed a nearly total absence of gonadal fat and a 70% reduction in subcutaneous fat (Fig. 1C and Table 1). The amount of BAT in

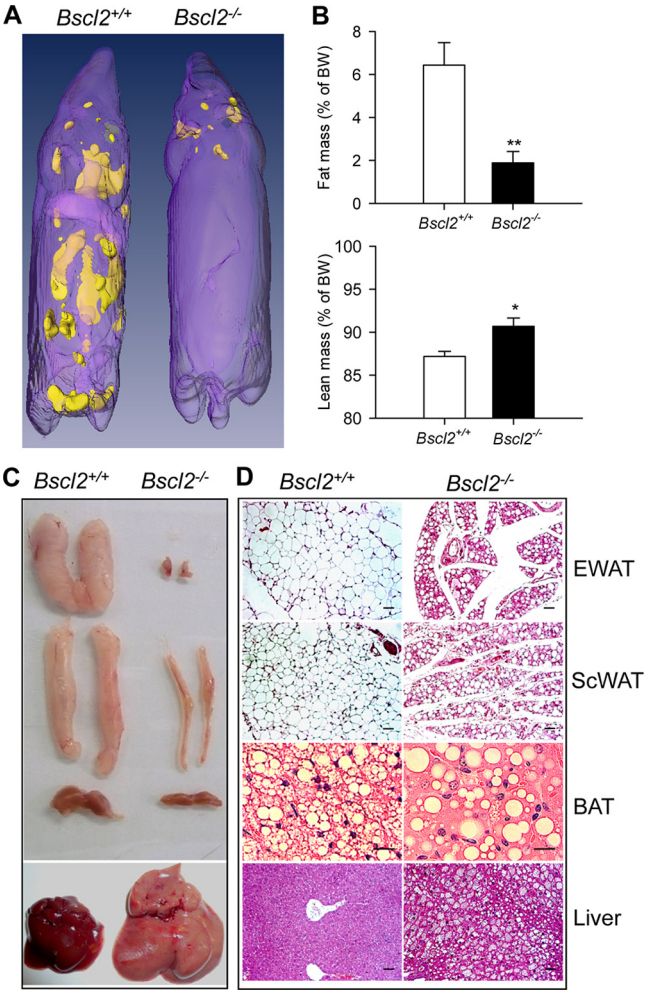

FIG 1 *Bscl2*$^{-/-}$ mice develop congenital generalized lipodystrophy. (A) 3D reconstruction of magnetic resonance imaging of the 12-week-old male wild-type and *Bscl2*$^{-/-}$ mice, with yellow color indicating fat. (B) EchoMRI analysis indicated the total fat mass and lean mass in 8-week-old male wild-type and *Bscl2*$^{-/-}$ mice ($n = 8$). Data were normalized to body weight (BW). *, $P < 0.05$; **, $P < 0.005$. (C and D) Gross appearances (C) and histology (D) of epididymal white fat pad (EWAT), subcutaneous white fat pad (ScWAT), interscapular brown fat pad (BAT), and liver of 12-week-old wild-type and *Bscl2*$^{-/-}$ mice. Sections of paraffin-fixed tissues were stained with hematoxylin-eosin and examined by light microscopy. Scale bar, 20 μm.

Bscl2$^{-/-}$ mice was also smaller than that in wild-type mice (Fig. 1C). Like type 2 CGL patients (3) and *Agpat2*$^{-/-}$ mice, another CGL type 1 model (12), *Bscl2*$^{-/-}$ mice have enlarged visceral organs (liver, kidneys, heart, and spleen) and a longer small intestine compared with wild-type mice (Table 1). Histology of the residual EWAT and ScWAT revealed a marked decrease in adipocyte size, with mostly unilocular LDs (Fig. 1D). Despite a pronounced reduction in the size of the EWAT and ScWAT depots, the total DNA content of the whole individual WAT depots was reduced by only ~50% (see Fig. S1F in the supplemental material), consistent with the decrease in WAT mass being the result of a reduction in both adipocyte size and number. The BAT in *Bscl2*$^{-/-}$ mice had largely lost the multilocular LD structure and contained few small LDs interspersed with occasional giant ones (Fig. 1D). The liver of *Bscl2*$^{-/-}$ mice was markedly steatotic (Fig. 1D and Table 1). The

TABLE 1 Phenotypic comparison of wild-type and *Bscl2*$^{-/-}$ mice[a]

Characteristic	Value for mouse of indicated sex and genotype			
	Male		Female	
	Wild type	*Bscl2*$^{-/-}$	Wild type	*Bscl2*$^{-/-}$
Body wt (g)	26.82 ± 1.57	30.3 ± 1.01	23.01 ± 1.06	21.7 ± 0.49
Organ measurement				
EWAT (mg)	360 ± 87	10 ± 0.9**	480 ± 90	15 ± 1.7**
ScWAT (mg)	250 ± 34	89 ± 22**	310 ± 50	42 ± 5.5*
BAT (mg)	72 ± 3	44 ± 7*	62 ± 5	43 ± 2*
Liver (g)	1.24 ± 0.048	2.21 ± 0.22**	0.94 ± 0.08	1.44 ± 0.07**
Heart (mg)	112 ± 7	160 ± 7**	94 ± 3	111 ± 4*
Spleen (mg)	70 ± 3	126 ± 8**	84 ± 7	132 ± 7*
Intestine (cm)	33.4 ± 1.95	41.6 ± 2.16*	37.3 ± 0.76	44.6 ± 1.54*
Kidney (mg)	330 ± 7	424 ± 18**	235 ± 9	250 ± 11
Leptin (ng/ml)	8.37 ± 2.1	1.38 ± 1.6**	5.33 ± 1.5	2.34 ± 0.43**
Adiponectin (ng/ml)	14.89 ± 2.17	2.17 ± 0.29**	21.7 ± 2.5	3.96 ± 0.36**
Liver TAG (mg/g)	3.9 ± 0.63	16.7 ± 5.3**	7.02 ± 0.96	14.7 ± 1.6**
Food intake (kcal/kg/h)	16.28 ± 1.66	21.79 ± 1.87*	ND	ND

[a] Mice (12 weeks of age) were fed with chow diet and sacrificed in the nonfasted state. Data were presented as means ± standard errors. *, $P < 0.05$; **, $P < 0.005$ (between the wild-type and *Bscl2*$^{-/-}$ mice in each sex group [$n = 6$ to 8]). EWAT, epididymal and perigonadal white adipose tissue; ScWAT, subcutaneous white adipose tissue; BAT, brown adipose tissue; TAG, triacylglycerol; ND, not determined.

mouse plasma leptin and adiponectin levels were greatly reduced, probably as a result of the marked deficiency of fat depots in these animals (Table 1). The hypoleptinemia likely contributed to hyperphagia, as male *Bscl2*$^{-/-}$ mice consumed 33% more calories than wild-type controls (Table 1).

***Bscl2*$^{-/-}$ mice are prodiabetic, with insulin resistance but without hyperlipidemia.** CGL patients usually have hyperacylglycerolemia (38). Interestingly, the levels of plasma triacylglycerol (TAG), nonesterified fatty acid (NEFA), and glycerol (collected at an arbitrarily selected time [10 a.m.], referred to here as "random") in *Bscl2*$^{-/-}$ and wild-type mice were similar; the levels became much lower in *Bscl2*$^{-/-}$ mice after they were subjected to 4 h and 24 h of fasting (Fig. 2A and B; see also Fig. S1G in the supplemental material). Random glucose and insulin levels were significantly elevated in *Bscl2*$^{-/-}$ mice by 10 weeks of age (Fig. 2C and D). After a 4-h fast, plasma glucose dropped by 50%, while insulin fell markedly but remained significantly higher in *Bscl2*$^{-/-}$ than in wild-type mice (Fig. 2C and D). Glucose and insulin levels went down further as the result of a 24-h fast in both genotypes. When the 24-h-fasted mice were refed regular chow for 6 h, the plasma TAG, NEFA, glycerol, glucose, and insulin levels rebounded in both groups but reached much higher levels in *Bscl2*$^{-/-}$ mice (Fig. 2; see also Fig. S1G in the supplemental material). These data strongly suggest that the lipodystrophic *Bscl2*$^{-/-}$ mice are prodiabetic with insulin resistance but develop no basal hypertriacylglycerolemia as seen in CGL patients (38) and other CGL mouse models such as *Agpat2*$^{-/-}$ mice (12).

Bscl2 is dispensable for initiation of LD formation but essential for LD maintenance and terminal adipocyte differentiation. To determine what underlies the phenomenon of markedly reduced body fat in *Bscl2*$^{-/-}$ mice, we examined the role of Bscl2 in directed differentiation of both murine embryonic fibroblasts (MEFs) and stromal vascular cells (SVCs) into adipocytes *in vitro*. We first detail our findings in MEFs and present the data from SVCs in a subsequent section.

Morphological examination showed that the early phase of adipocyte differentiation in *Bscl2*$^{-/-}$ MEFs was largely indistinguishable from that of wild-type MEFs. LD formation occurred relatively normally at day 3 (3 days after adding differentiation media) and day 4 but became defective by days 5 and 6, when most

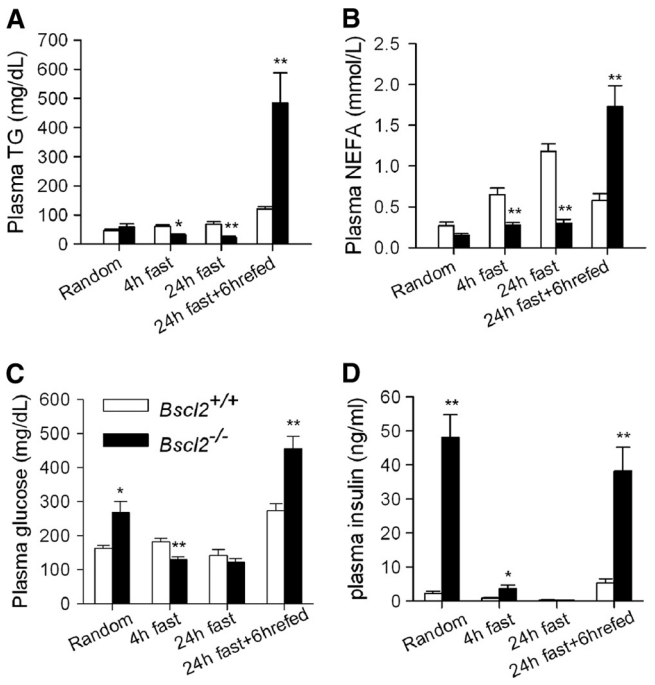

FIG 2 *Bscl2*$^{-/-}$ mice have altered lipid and carbohydrate homeostasis. Plasma triacylglycerol (TAG) (A), nonesterified fatty acids (NEFA) (B), glucose(C), and insulin (D) were measured in 10-week-old male wild-type and *Bscl2*$^{-/-}$ mice at a randomly selected time (10 a.m.) or after a 4-h fast, 24-h fast, and 24-h fast followed by refeeding (6 h) with normal chow diet ($n = 8$ to 10 each). *, $P < 0.05$; **, $P < 0.005$ (for comparisons of *Bscl2*$^{+/+}$ and *Bscl2*$^{-/-}$ mice under same conditions).

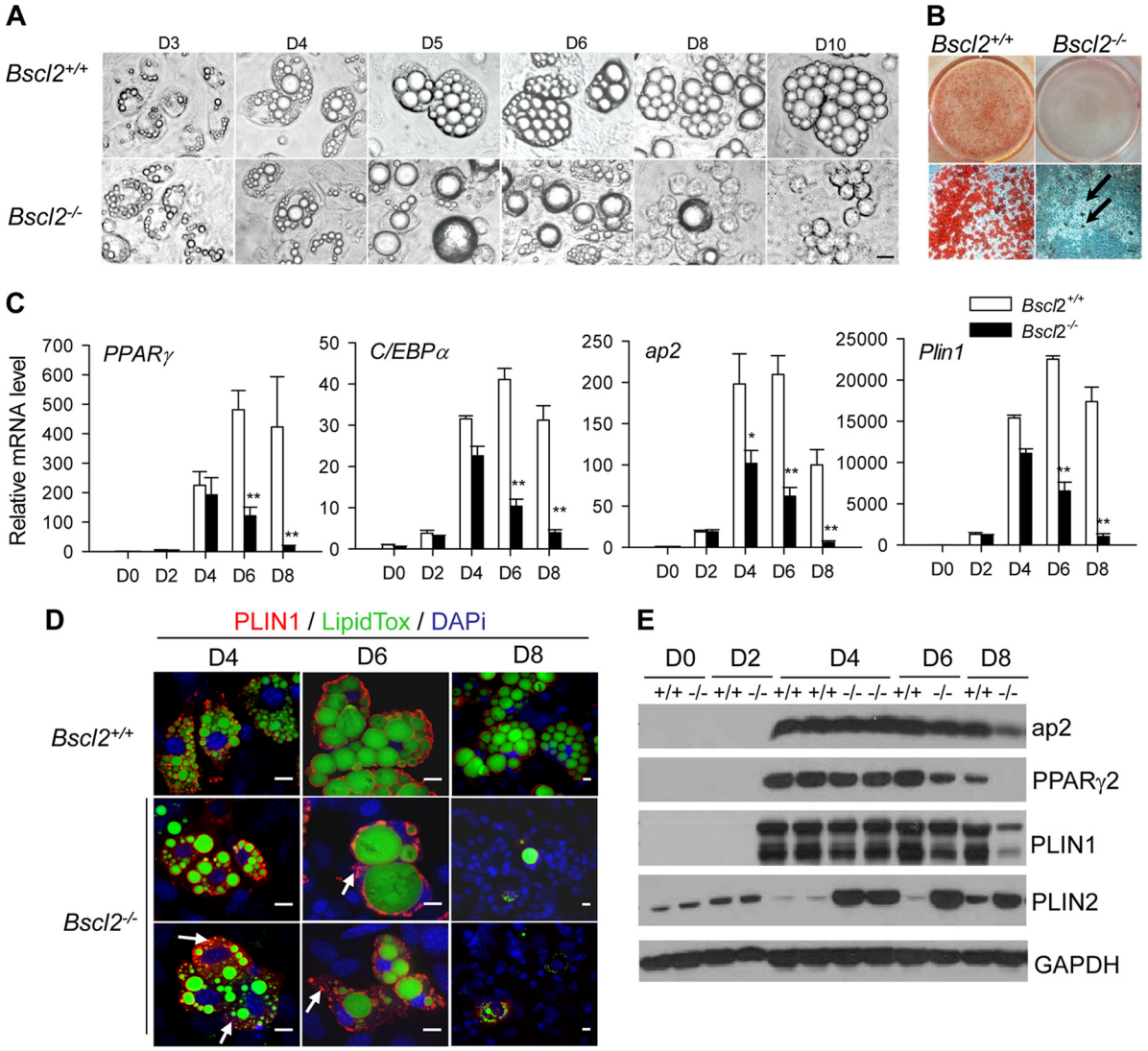

FIG 3 Bscl2 is essential in lipid droplet and mature adipocyte maintenance *in vitro*. (A) Comparison of lipid droplet formation and changes during different days (day 3 [D3] to D10) of differentiation in wild-type and *Bscl2*$^{-/-}$ MEFs using a light microscope. Scale bar, 10 μm (all images). (B) Oil-Red O staining of day 8 wild-type and *Bscl2*$^{-/-}$ MEF adipocytes. Scale bar, 10 μm. Arrows indicate the very few Oil-Red O-stained differentiated cells in *Bscl2*$^{-/-}$ MEFs at day 8. (C) Quantitative RT-PCR analyses of master adipocyte differentiation transcription factors (PPARγ and C/EBPα) as well as mature adipocyte markers (ap2 and Plin1) in wild-type and *Bscl2*$^{-/-}$ MEFs undergoing differentiation. Data were normalized to cyclophilin A and are expressed as relative fold changes compared to the wild type at day 0 (the day when the differentiation medium was added). *, $P < 0.05$; **, $P < 0.005$ (versus wild-type on the same day). (D) Immunofluorescent staining of PLIN1 and LipidTOX (a specific neutral lipid dye) in MEFs at day 4, day 6, and day 8 after differentiation. Arrows indicate microlipid droplets that were mainly stained by PLIN1 in *Bscl2*$^{-/-}$ MEF cells. Scale bar, 10 μm. (E) Western blot analysis of whole-cell lysates harvested from wild-type and *Bscl2*$^{-/-}$ MEFs at different days of differentiation. Identical amounts of proteins were loaded, and GAPDH was used as a loading control.

of the *Bscl2*$^{-/-}$ MEF adipocytes contained only one or two supersized LDs instead of the numerous normal-sized LDs seen in wild-type cells. By day 8, almost all *Bscl2*$^{-/-}$ MEF adipocytes had turned into rounded cells that were devoid of intracellular LDs (Fig. 3A). Oil-Red O staining of day 8 differentiated MEFs confirmed that, in contrast to wild-type MEF adipocytes, only ~5% of the *Bscl2*$^{-/-}$ MEFs contained LDs (Fig. 3B). Consistent with the morphological aberrations, the transcripts for PPARγ and C/EBPα and the lipid droplet protein (LDP) PLIN1 at both day 2 and day 4 were expressed at similar levels in the *Bscl2*$^{-/-}$ and wild-type MEFs. The adipocyte marker ap2 was expressed at the same level at day 2 but lagged at day 4 in the *Bscl2*$^{-/-}$ MEFs. However, in the absence of Bscl2, the mRNA expression level of these markers was not sustained beyond day 4; instead, the level fell precipitously at day 6 and was at almost undetectable levels at day 8, suggesting that loss of Bscl2 adversely affects the maturation of adipocytes beyond the first 2 to 4 days of differentiation (Fig. 3C). The mRNA expression of other genes involved in glucose transport (*glut4*), TAG synthesis (*Agpat2*), and lipolysis (*Atgl* and *Hsl*) followed a pattern similar to that seen with the master transcription factors PPARγ and C/EBPα (see Fig. S2A in the supplemental material). Therefore, the day 8 *Bscl2*$^{-/-}$ cells were phenotypically distinct from mature adipocytes, having lost the adipocyte-specific transcription factors and markers and all neutral lipid-containing LDs.

We also monitored the dynamic changes in LDs from day 4 to

day 8 by immunofluorescence microscopy using a combination of PLIN1 immunostaining, which coats the surface of mature LDs (Fig. 3D [red]), and LipidTOX, a dye that specifically lights up the core TAG of LDs (Fig. 3D [green]). Corroborating the light microscopy data (Fig. 3A) and PLIN1 gene expression data (Fig. 3C), the initiation of differentiation and LD accumulation in MEFs appeared only mildly perturbed at day 4 in the *Bscl2*$^{-/-}$ MEFs: there was an increased number of micro-LDs (marked by arrows in Fig. 3D) in *Bscl2*$^{-/-}$ MEFs compared to wild-type controls. On day 6, in contrast to the well-organized LDs in wild-type MEFs, most differentiating *Bscl2*$^{-/-}$ MEFs exhibited one or two supersized LDs (up to ~30 μm in diameter) together with a few neighboring micro-LDs. By day 8, few PLIN1-positive cells or LipidTOX-positive LDs were detectable, indicating that most *Bscl2*$^{-/-}$ MEFs failed to differentiate into mature adipocytes (Fig. 3D; note the blue DAPI [4′,6′diamidino-2-phenylindole] staining of nuclei). There was, however, no major difference in ER apposition and mitochondrial number and association with LDs in day 4 and day 6 wild-type or *Bscl2*$^{-/-}$ MEFs other than the abnormal LD size and distribution in the latter (see Fig. S2B in the supplemental material).

In parallel with changes in their mRNA, the levels of protein expression of mature adipocyte markers ap2, PPARγ2, and PLIN1 went up on day 4 in both *Bscl2*$^{-/-}$ and wild-type MEFs. They came down significantly on day 6 and were extremely low or undetectable on day 8 in *Bscl2*$^{-/-}$ MEFs though they remained high in wild-type cells (Fig. 3E). In contrast to these adipocyte marker proteins, the differentiating *Bscl2*$^{-/-}$ MEFs expressed much larger amount of PLIN2 from day 4 to day 8 compared to the wild-type differentiating MEFs (Fig. 3E). It is noteworthy that PLIN1 and PLIN2 were colocalized in a large fraction of the day 6 *Bscl2*$^{-/-}$ MEFs whereas wild-type day 6 MEFs expressed only PLIN1 protein (see Fig. S2C in the supplemental material). Therefore, ablation of Bscl2 dramatically modified the expression of the key adipogenic transcription factors such as PPARγ and C/EBPα and the pattern of expression of PAT family LDPs, as well as the size of LDs during adipocyte differentiation.

As there is evidence that Bscl2 is an ER resident protein (11, 26), we determined whether loss of Bscl2 causes ER stress and apoptosis, which might contribute to the failure of *Bscl2*$^{-/-}$ MEFs to become mature adipocytes at a late stage of differentiation. We quantified the mRNA expression of ER stress marker proteins Chop and Bip and found no difference in their expression in *Bscl2*$^{-/-}$ cells compared with wild-type cells either at day 4 to day 6, when the cells were undergoing dynamic changes, or later, at day 8, when most *Bscl2*$^{-/-}$ MEFs had turned into rounded cells (see Fig. S3A and S3B in the supplemental material). A highly sensitive Caspase 3/7 activity assay demonstrated a minimal 1.2-fold increase in activity *Bscl2*$^{-/-}$ cells at day 10, when ~95% of the MEFs had become rounded cells (see Fig. S3C in the supplemental material). Furthermore, terminal deoxynucleotidyltransferase-mediated dUTP-biotin nick end labeling (TUNEL) staining of day 10 MEFs revealed no evident apoptosis in either wild-type or *Bscl2*$^{-/-}$ cells (see Fig. S3D in the supplemental material), suggesting that ER stress-related apoptosis was not the culprit responsible for the aborted adipogenesis in the absence of Bscl2.

Enhanced lipolysis underlies the depletion of TAG in differentiating *Bscl2*$^{-/-}$ MEFs. We measured the rate of lipolysis in differentiating MEFs at day 4, a stage at which *Bscl2*$^{-/-}$ and wild-type MEFs displayed mostly comparable features of adipocyte differentiation. The amount of NEFA and glycerol from *Bscl2*$^{-/-}$ MEFs in media under basal conditions was almost double that of wild-type MEFs (Fig. 4A). Addition of β3 adrenergic agonist CL 316243 stimulated lipolysis in both genotypes to similar extents.

We next monitored glycerol content in media and TAG content in the cells during the 10 days of induced adipocyte differentiation. On day 4, *Bscl2*$^{-/-}$ MEFs released more than twice the amount of glycerol in the media as the wild-type cells. The exaggerated release of glycerol continued to plague *Bscl2*$^{-/-}$ MEFs on day 6, returning to a level similar to that of the wild type only on day 8 and going down even further on day 10, when most of the *Bscl2*$^{-/-}$ cells were depleted of TAG and turned into rounded cells whereas the wild-type MEFs had become mature adipocytes (Fig. 4B, top panel). The intracellular TAG content in *Bscl2*$^{-/-}$ MEFs increased but was about half of that in wild-type cells on day 4 and day 6, and it fell to an almost undetectable level on day 8 and day 10, consistent with their morphological transition to rounded cells with essentially no lipids (Fig. 4B, bottom panel). Notably, rates of TAG synthesis of day 4 wild-type and *Bscl2*$^{-/-}$ MEFs were similar (see Fig. S4A in the supplemental material).

Lipase inhibitors, but not a PPARγ agonist, rescue the adipocyte differentiation defect in *Bscl2*$^{-/-}$ MEFs. We examined the potential role of upregulated lipolysis in the abnormal adipose differentiation of *Bscl2*$^{-/-}$ MEFs by adding E600, a TAG lipase inhibitor, to MEF cultures beginning on day 4. Addition of E600 to the differentiating MEFs on day 4 effectively inhibited TAG hydrolysis, suppressing the glycerol released to predifferentiation levels in both wild-type and *Bscl2*$^{-/-}$ cells, while it restored cellular TAG content in *Bscl2*$^{-/-}$ cells on day 6, day 8, and day 10 (Fig. 4B). Importantly, lipase inhibition not only rescued the TAG accumulation but also restored the mRNA expression of PPARγ, C/EBPα, PLIN1, and ap2 in day 10 *Bscl2*$^{-/-}$ MEFs to a level similar to that of E600-treated wild-type MEFs at day 10 (Fig. 4C). We note that E600 treatment also moderately stimulated TAG accumulation and expression of PPARγ, C/EBPα, PLIN1, and ap2 transcripts in day 10 wild-type MEFs, underscoring an integral role of controlled lipolysis in regulating normal adipocyte differentiation. Western blotting corroborated the restoration of PPARγ2, ap2, and PLIN1A protein expression in day 8 and day 10 differentiated *Bscl2*$^{-/-}$ MEFs treated with E600 (see Fig. S4B in the supplemental material). Immunofluorescence staining further showed that lipase inhibition rescued adipocyte differentiation in day 10 *Bscl2*$^{-/-}$ MEFs as indicated by the restoration of PLIN1-coated LDs in *Bscl2*$^{-/-}$ adipocytes to a level similar to that seen with wild-type MEFs with E600 treatment (Fig. 4D, right panels). Use of another TAG lipase inhibitor, DEUP, similarly rescued adipocyte differentiation in *Bscl2*$^{-/-}$ MEFs (data not shown).

We next examined whether a PPARγ agonist would rescue adipocyte differentiation of *Bscl2*$^{-/-}$ MEFs as we had previously demonstrated in Bscl2 knockdown 3T3-L1 cells (11). The addition of the PPARγ agonist pioglitazone in the culture medium led to enhanced adipocyte differentiation and TAG accumulation in wild-type MEFs, as indicated by Oil-Red O staining (Fig. 5A) and a direct enzymatic assay (Fig. 5B). In the absence of E600 treatment, addition of pioglitazone to *Bscl2*$^{-/-}$ MEFs only modestly increased TAG accumulation by ~30% compared to vehicle alone. Only with the addition of E600 could TAG accumulation be restored to a level similar to that of wild-type MEF adipocytes (Fig. 5A and B). Adding pioglitazone together with E600 did not further enhance TAG accumulation in the WT or *Bscl2*$^{-/-}$ MEFs. The

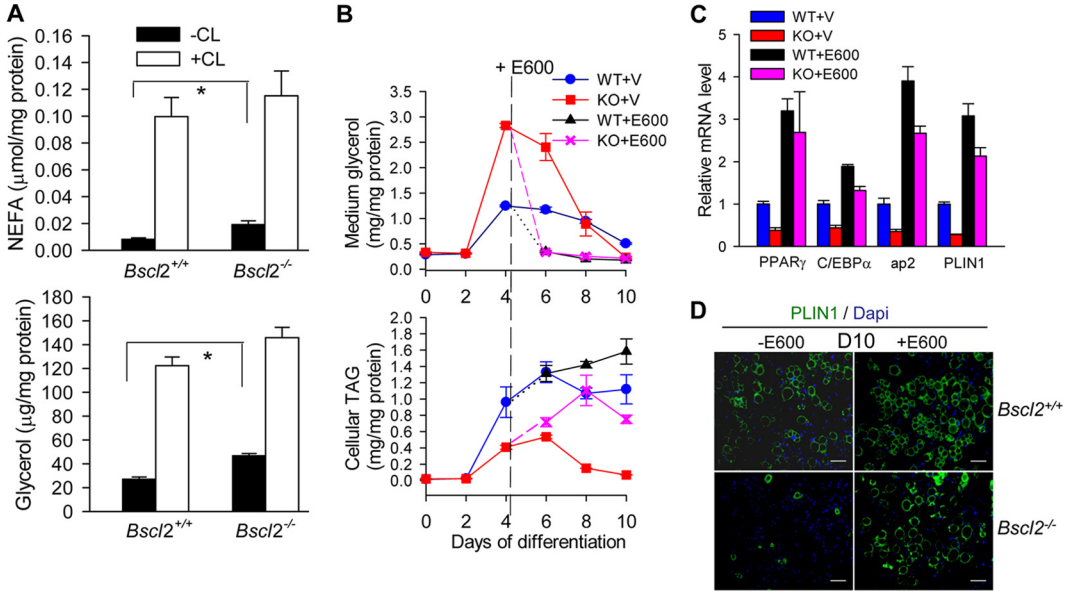

FIG 4 Enhanced lipolysis leads to aborted adipocyte differentiation in *Bscl2*$^{-/-}$ MEFs which could be restored by lipase inhibitors. (A) NFFA and glycerol release in day 4 differentiating wild-type and *Bscl2*$^{-/-}$ MEFs under conditions of basal and CL 316243-stimulated lipolysis *in vitro*. Data were normalized to cellular protein levels. *, $P < 0.05$; **, $P < 0.005$. (B) Medium glycerol as well as intracellular TAG levels were assessed at the indicated days of differentiation in the wild-type (WT) and *Bscl2*$^{-/-}$ (KO) MEFs. Data were normalized to cellular protein levels. Vehicle (V) or 200 μM E600, a lipase inhibitor, was added at day 4 and afterward. (C) Quantitative RT-PCR analyses of mRNA expression of PPARγ, C/EBPα, ap2, and Plin1 in day 10 wild-type (WT) and *Bscl2*$^{-/-}$ (KO) MEFs with vehicle (V) or E600 treatment. Data were normalized to cyclophilin A and are expressed as relative fold changes compared to the wild type treated with vehicle. (D) Immunofluorescence staining with anti-PLIN1 antibody on day 10 of *Bscl2*$^{+/+}$ and *Bscl2*$^{-/-}$ MEFs with (+) or without (−) E600 treatment. Scale bar, 50 μm.

differential effect of E600 and pioglitazone was correlated with the differential lipolysis rate, as the amount of glycerol released was the highest in day 6 to day 14 differentiated *Bscl2*$^{-/-}$ MEFs treated with pioglitazone only (open squares in Fig. 5C), whereas E600 successfully inhibited lipolysis in all treatment groups (Fig. 5C). Therefore, enhanced lipolysis plays a dominant role in the differentiation defect of *Bscl2*$^{-/-}$ MEFs, which is restored only by a lipase inhibitor but not to a significant extent by a PPARγ agonist.

Loss of Bscl2 results in increased cAMP-dependent PKA-stimulated lipolysis. To gain insight into the possible lipolytic pathway activated in the absence of Bscl2, we analyzed by Western blotting the major proteins that are known to regulate lipolysis. We found no difference in total PLIN1A protein and a minor difference at day 4 but modestly lower levels at day 6 for HSL and ATGL in *Bscl2*$^{-/-}$ compared to wild-type MEFs (Fig. 6A). This is in agreement with their respective mRNA levels (Fig. 3; see also S2A in the supplemental material). Interestingly, however, HSL phosphorylation at serine 563 and PLIN1A phosphorylation at serine 517 were both upregulated in the basal state in day 4 and day 6 differentiating *Bscl2*$^{-/-}$ MEFs (Fig. 6A). Those two sites are known to be phosphorylated by protein kinase A (PKA) in a cAMP-dependent manner. The ratio of phosphorylated to total protein increased ~1.9-fold for HSL and 2.4-fold for PLIN1A at day 4 (Fig. 6B). Moreover, an even larger amount of total and phosphorylated HSL and total ATGL was localized in the LD fraction of day 4 *Bscl2*$^{-/-}$ MEFs compared to wild-type MEFs (Fig. 6C). The enrichment of these proteins in LDs is a key event that occurred only in normal adipocytes during stimulated lipolysis (30, 31). Interestingly, PLIN2, which is normally not present in the mature adipocytes, was recruited to the LDs of the *Bscl2*$^{-/-}$ MEFs at day 4 (Fig. 6C). Together, these data suggest that there is an enhanced basal lipolysis in the differentiating *Bscl2*$^{-/-}$ MEFs which prevents these cells from becoming fully mature adipocytes.

We next examined whether the increased lipolysis in differentiating *Bscl2*$^{-/-}$ MEFs occurred via a cAMP-dependent PKA pathway, as two of its substrates showed elevated phosphorylation. The cellular cAMP content in day 4 *Bscl2*$^{-/-}$ MEFs was indeed ~1.65-fold higher than that in the wild type (Fig. 6D). The addition of H89, a potent PKA inhibitor, partially rescued the cellular TAG accumulation in *Bscl2*$^{-/-}$ MEFs at day 12 (Fig. 6E). Despite the still substantially lower cellular TAG content in H89-treated *Bscl2*$^{-/-}$ cells, PKA inhibition partially restored the protein expression of PPARγ2 and PLIN1, whereas expression of ap2 in *Bscl2*$^{-/-}$ MEFs at day 12 was largely restored compared to the wild type with or without H89 treatment (Fig. 6F), suggesting that more mature adipocytes were sustained in H89-treated *Bscl2*$^{-/-}$ MEFs. These data further support the conclusion that abnormal constitutively elevated cAMP-dependent PKA-stimulated lipolysis in the differentiating *Bscl2*$^{-/-}$ MEFs underlies the impaired adipogenesis, an aberrant process which can be partially reversed by PKA inhibition.

In vitro adipogenesis of isolated stromal vascular cells (SVCs) reproduced essentially all the major findings determined using MEFs. The mRNA expression of PPARγ and Plin1 in differentiating *Bscl2*$^{-/-}$ SVCs followed dynamic patterns similar to those seen in *Bscl2*$^{-/-}$ MEFs compared to their wild-type counterparts (see Fig. S5A in the supplemental material). Basal lipolysis is higher in day 4 differentiating *Bscl2*$^{-/-}$ SVCs than in wild-type SVCs (see Fig. S5B in the supplemental material). They also failed to become mature adipocytes on day 10, and this failure was rescued by treat-

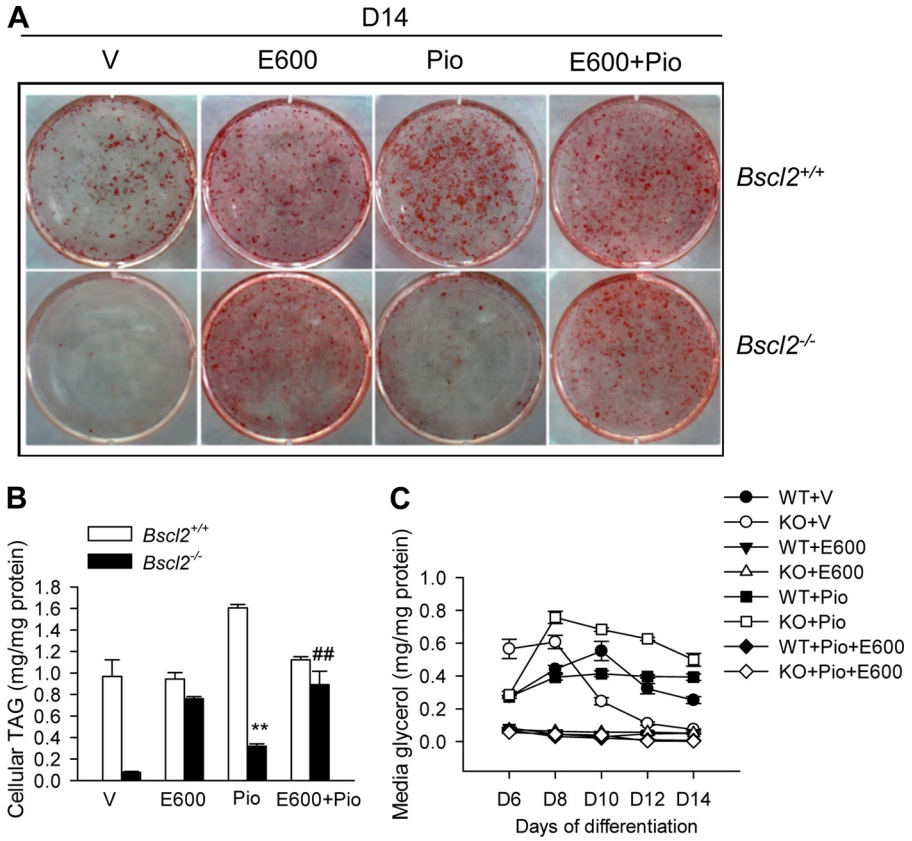

FIG 5 A PPARγ agonist could not significantly rescue the adipocyte differentiation defect in *Bscl2*$^{-/-}$ MEFs. (A) Oil-Red O staining of day 14 wild-type and *Bscl2*$^{-/-}$ MEFs with E600 (from day 4) and/or pioglitazone (from day 0) treatment. (B and C) Intracellular TAG levels at day 14 (B) and medium glycerol (from day 6 to day 14) (C) were assessed at the indicated days of differentiation in the wild-type (WT) and *Bscl2*$^{-/-}$ (KO) MEFs. Data were normalized to cellular protein levels. Piglitazone (Pio) (1 μM) was included throughout the differentiation, while vehicle (V) or 200 μM E600 was added from day 4 and afterward. **, $P < 0.005$ (versus WT with Pio); ##, $P < 0.05$ (versus KO with Pio treatment alone).

ment with lipase inhibitor E600 (see Fig. S5C in the supplemental material). Moreover, the intracellular cAMP level was higher in day 4 differentiating *Bscl2*$^{-/-}$ SVCs than in the wild type (see Fig. S5D in the supplemental material). The increased cAMP-mediated PKA activation was further confirmed by elevated phosphorylation of HSL at PKA sites in day 4 differentiating *Bscl2*$^{-/-}$ SVCs (see Fig. S5E in the supplemental material). These findings further support the conclusion that activated lipolysis blunts adipocyte differentiation in both *Bscl2*$^{-/-}$ SVCs and MEFs.

Chronic activation of cAMP/PKA signaling impairs wild-type MEF differentiation. To further examine whether unbridled stimulated lipolysis downstream of cAMP/PKA signaling compromises adipocyte differentiation, we exposed differentiating wild-type MEFs (from day 4) to either an adenyl-cyclase agonist (forskolin) or a specific phosphodiesterase inhibitor (IBMX) to increase the cellular cAMP content. As expected, forskolin and IBMX markedly stimulated lipoysis, as evidenced by greatly increased glycerol release in wild-type MEFs (from day 6 to day 10) (Fig. 7A). By day 10, cellular TAG levels were reduced by ~60% in both forskolin- and IBMX-treated cells in comparison with vehicle-treated cells (Fig. 7B). The cAMP/PKA activation was accompanied by a marked downregulation in the mRNA expression of PPARγ and C/EBPα as well as their downstream targets, glut4 and PLIN1 (Fig. 7C). These data further support a critical role of well-controlled cAMP-mediated lipolysis in maintaining normal adipocyte differentiation.

Deletion of *Bscl2* leads to higher lipolysis *in vivo*. Due to the nearly total absence of adipose tissue, *Bscl2*$^{-/-}$ mice had lower basal NEFA and glycerol levels and failed to mount a significant response to β-adrenergic agonist-induced lipolysis (Fig. 8A). However, when we normalized the serum NEFA and glycerol levels to the absolute amounts of fat tissues *in vivo* (e.g., to the total fat masses measured by MRI), we observed data consistent with an increased rate of basal lipolysis in *Bscl2*$^{-/-}$ mice *in vivo* (Fig. 8B), although CL 316243-stimulated lipolysis was still blunted due to limited adipose TAG available for stimulation. We also performed *ex vivo* lipolysis from EWAT explants and found significantly higher basal lipolysis when values were normalized to the total absolute explant weights in fat pads from *Bscl2*$^{-/-}$ mice (Fig. 8C). We tried to measure lipolysis using isolated adipocytes but found that it was not possible to isolate the very scant and smaller adipocytes, which could not be efficiently fractionated by centrifugation.

Gene expression changes in the residual EWAT of *Bscl2*$^{-/-}$ mice confirmed *in vitro* findings. By qPCR, the residual EWAT of *Bscl2*$^{-/-}$ mice was unexpectedly found to express levels of mature adipocyte marker genes, including the ap2, PPARγ, and C/EBPα genes, that were similar to wild-type levels. In contrast, however,

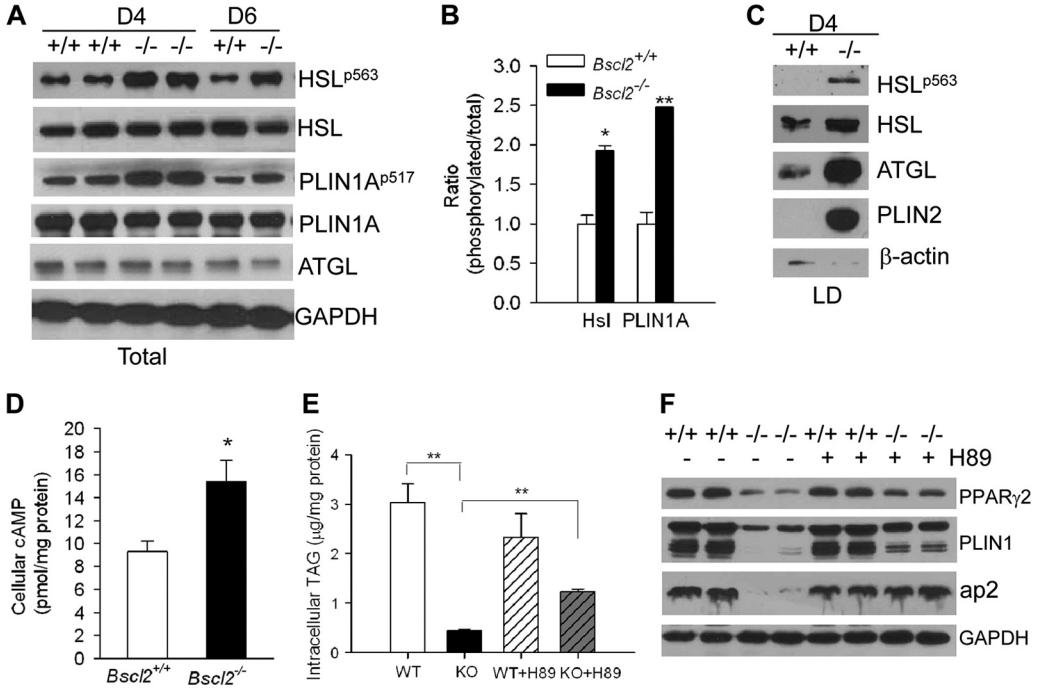

FIG 6 Increased cAMP-dependent PKA-stimulated lipolysis impairs adipocyte differentiation. (A) Western blot analyses of lipolytic proteins in day 4 and day 6 wild-type (+/+) and *Bscl2*$^{-/-}$ (−/−) MEF whole-cell lysates. Antibodies against phospho-specific proteins as well as total proteins were used as indicated. (B) Semiquantitative analysis of ratio of phosphorylated to total HSL and PLIN1A in the day 4 differentiating wild-type and *Bscl2*$^{-/-}$ MEFs. (C) Western blot analyses of lipolytic proteins in isolated intracellular LDs from day 4 differentiating wild-type (+/+) and *Bscl2*$^{-/-}$ (−/−) MEFs, with β-actin as a loading control. (D) Intracellular cAMP levels in day 4 differentiating wild-type and *Bscl2*$^{-/-}$ MEF cells. Data were normalized to total cytosolic proteins. (E) The intracellular TAG levels in day 12 wild-type (WT) and *Bscl2*$^{-/-}$ (KO) MEF cells with vehicle (+V) or H89 (+H89) treatment. H89 (10 μM) was added at day 4. Data were normalized to total cellular proteins. (F) Western blot analyses of mature adipocyte markers in day 12 differentiated wild-type (+/+) and *Bscl2*$^{-/-}$ (−/−) MEFs with (+) or without (−) H89 treatment. Identical amounts of proteins were loaded, and GAPDH was used as a loading control.

the expression of Pref1 (a preadipocyte marker) was markedly downregulated (by 83%; Fig. 9A). The mRNA expression of C/EBPβ, an important transcription factor required for the early stage of adipogenesis, was increased by about 2.5-fold. These observations suggest that preadipocytes were depleted *in vivo* in EWAT of *Bscl2*$^{-/-}$ mice, as more of them had been driven to undergo early adipocyte differentiation in response to less-than-optimal terminal adipocyte differentiation and/or maintenance. Interestingly, UCP1 expression, which was previously reported to be greatly regulated by cAMP-mediated PKA activation (36), was increased in the residual EWAT by >2,000-fold in *Bscl2*$^{-/-}$ mice (Fig. 9B). Transcripts for two other BAT-specific genes, the Cidea and Elovl3 genes, as well as fatty acid oxidation and mitochondrion-related genes (CPT1 and CytC genes) were also markedly increased, though PGC1α and PGC1β levels were not changed (Fig. 9C). In combination with the changes in histology (Fig. 1C), these data suggest that deletion of Bscl2 induced the development of a brown adipose tissue-like phenotype in the residual EWAT in *Bscl2*$^{-/-}$ mice.

When analyzed at the protein level, UCP1, which is normally not detectable in WAT, was readily detected by Western blotting in the EWAT of *Bscl2*$^{-/-}$ mice (Fig. 9D), in keeping with the

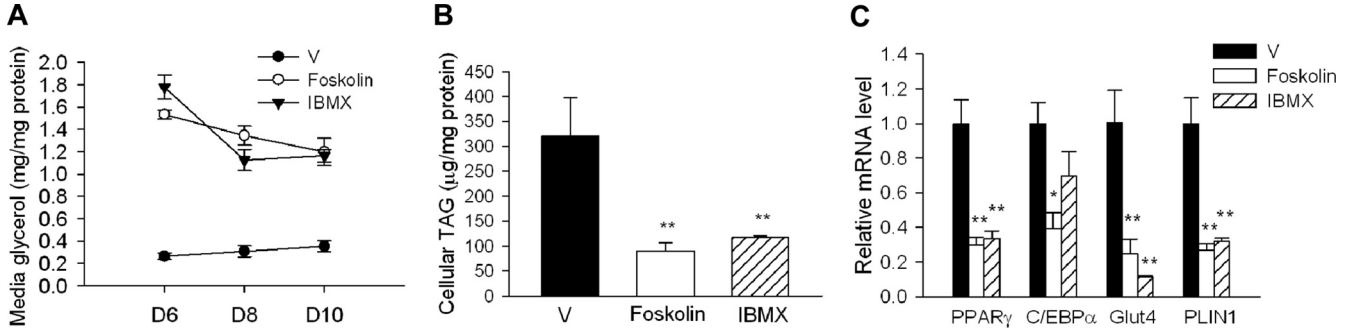

FIG 7 Chronic activation of cAMP/PKA signaling impairs wild-type MEF differentiation. (A) The medium glycerol levels in day 6 to day 10 wild-type MEF cells chronically treated with vehicle dimethyl sulfoxide (DMSOJ) (V), forskolin (10 μM), or IBMX (0.5 mM) from day 4. Data were normalized to total cellular proteins. **, $P < 0.005$. (B and C) The intracellular TAG levels (B) and mRNA expression (C) in day 10 wild-type (WT) MEF cells with chronic vehicle (V), forskolin (10 μM), or IBMX (0.5 mM) treatment from day 4. *, $P < 0.05$. **, $P < 0.005$.

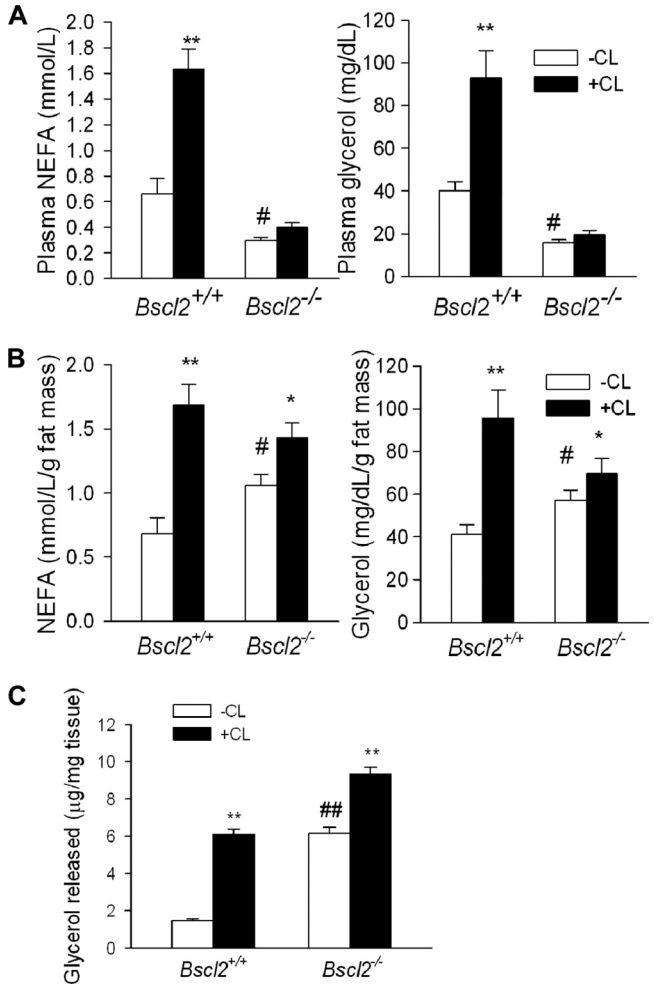

FIG 8 The EWAT of *Bscl2*$^{-/-}$ mice has higher lipolysis *in vivo* and *ex vivo*. (A and B) NFFA and glycerol release in 12-week-old male wild-type and *Bscl2*$^{-/-}$ mice ($n = 6$ each) under conditions of basal and CL 316243-stimulated lipolysis *in vivo* without normalization (A) and with normalization to total fat mass contents based on EchoMRI (B). (C) *Ex vivo* lipolysis of EWAT explants from wild-type and *Bscl2*$^{-/-}$ mice. EWAT fat explants were taken from 6-week-old male wild-type and *Bscl2*$^{-/-}$ mice. After intensive washing, lipolysis was performed with or without CL 316243 (+CL) for 2 h. The amounts of glycerol released were normalized to the explant wet weights. $n = 6$ each. *, $P < 0.05$; **, $P < 0.005$ [versus basal state (-CL) among the same genotype]; ##, $P < 0.005$ [versus wild-type mice at basal state (-CL)].

drastically increased level of its mRNA (Fig. 9B). The protein expression of total HSL and PLIN1 in the residual EWAT of *Bscl2*$^{-/-}$ mice was not different, and the phosphorylation of serine 563 at HSL showed only a trend to be higher than that of the wild type. However, PLIN2, which is normally barely detectable in mature EWAT (7), was massively upregulated in EWAT of *Bscl2*$^{-/-}$ mice compared to that of wild-type mice (Fig. 9D) in a manner similar to what we observed in differentiating *Bscl2*$^{-/-}$ cells *in vitro* (Fig. 3E).

cAMP/PKA-stimulated lipolysis in white adipocytes has been shown to acutely induce mitochondrial uncoupling and cellular energetics induced by fatty acids released by lipolysis (47). To further provide insight into why the residual EWAT of *Bscl2*$^{-/-}$ mice exhibits a BAT-like phenotype, we measured the oxygen consumption rate (OCR [aerobic respiration]) and extracellular acidification rate (ECAR [anaerobic respiration]) in day 4 differentiating wild-type and *Bscl2*$^{-/-}$ MEF adipocytes. *Bscl2*$^{-/-}$ MEF adipocytes exhibited a 35% higher OCR and 26% higher ECAR compared with *Bscl2*$^{+/+}$ MEFs (Fig. 9E and F), suggesting increased mitochondrial uncoupling. We failed to observe a consistent upregulation of expression of UCP1 and other mitochondrial genes in day 4 differentiating *Bscl2*$^{-/-}$ MEFs (data not shown), which could have been due to the dynamic turnover of *Bsc2*$^{-/-}$ differentiating adipocytes *in vitro*. Nevertheless, these data further suggest that enhanced cAMP/PKA-mediated lipolysis could have led to increased mitochondrial uncoupling, possibly contributing to the BAT-like phenotype in the EWAT of *Bscl2*$^{-/-}$ mice.

DISCUSSION

Targeted gene deletion of Bscl2 in mice is associated with a marked loss of fat, especially gonadal WAT. The lipodystrophic *Bscl2*$^{-/-}$ mice also display hyperinsulinemia, dyslipidemia, hepatic steatosis, and hyperphagia as well as enlarged liver, spleen, kidney, and heart and elongated small intestine, recapitulating the major phenotypic features of CGL type 2 patients. Sexual dimorphism was evident, as male mice were more severely affected than females (Table 1; see also Fig. S1E in the supplemental material). However, interestingly, the extent of adipose tissue loss in *Bscl2*$^{-/-}$ mice was less severe than in *Agpat2*$^{-/-}$ mice which have no detectable adipose tissue (12). Similarly, the rate of premature death of *Bscl2*$^{-/-}$ mice (21%) was lower than that of *Agpat2*$^{-/-}$ mice (~80%) (12). This is in direct contrast to the clinical phenotypes of the two CGL subtypes in humans, in which CGL type 2 individuals have a more severe loss of adipose tissue and earlier onset of diabetes as well as a higher incidence of premature death compared to CGL type 1 patients with AGPAT2 mutations (1, 3). The discrepancy may be due to the differential pathways these two genes are involved in and the relative importance of these pathways in human and mouse adipose tissue development. Meanwhile, the less severe adipose tissue loss and absence of hypertriglyceridemia or overt diabetes in *Bscl2*$^{-/-}$ mice compared to CGL2 humans suggests other differences between human and mouse physiologies.

The creation of the lipodystrophic *Bscl2*$^{-/-}$ mice provided us with a powerful model in which to investigate the pathophysiology that underlies CGL type 2 individuals and enabled us to examine the role of Bscl2 in adipocyte differentiation. We found that in differentiating *Bscl2*$^{-/-}$ cells, uncontrolled cAMP-dependent PKA-stimulated lipolysis depletes the cellular content of TAG, resulting in failure of LD maintenance and ultimately causing the cells to abort the adipocyte differentiation program. The principal players in the stimulated lipolysis pathway, HSL and PLIN1A, are highly phosphorylated at PKA sites in the total lysates of *Bscl2*$^{-/-}$ cells (Fig. 6A). In a situation resembling that of adipocytes stimulated by cAMP-dependent PKA activation (8, 40), the differentiating *Bscl2*$^{-/-}$ cells also recruit more lipolytic enzymes to the LDs, further accelerating lipolysis (Fig. 6C). Moreover, the dynamic changes of LD sizes and the abnormal expression of PAT family LDPs during *Bscl2*$^{-/-}$ cell differentiation further support the presence of ongoing and unbridled lipolysis.

Notably, the early-stage differentiating *Bscl2*$^{-/-}$ cells contain numerous dispersed microlipid droplets coated with PLIN1 (Fig. 3D). Similar microlipid droplets have been previously found in adipocytes chronically stimulated with β-adrenergic receptor agonists (10, 25) and to occur with PLIN1 phosphorylation via PKA activation (27). The much smaller LDs were also observed in

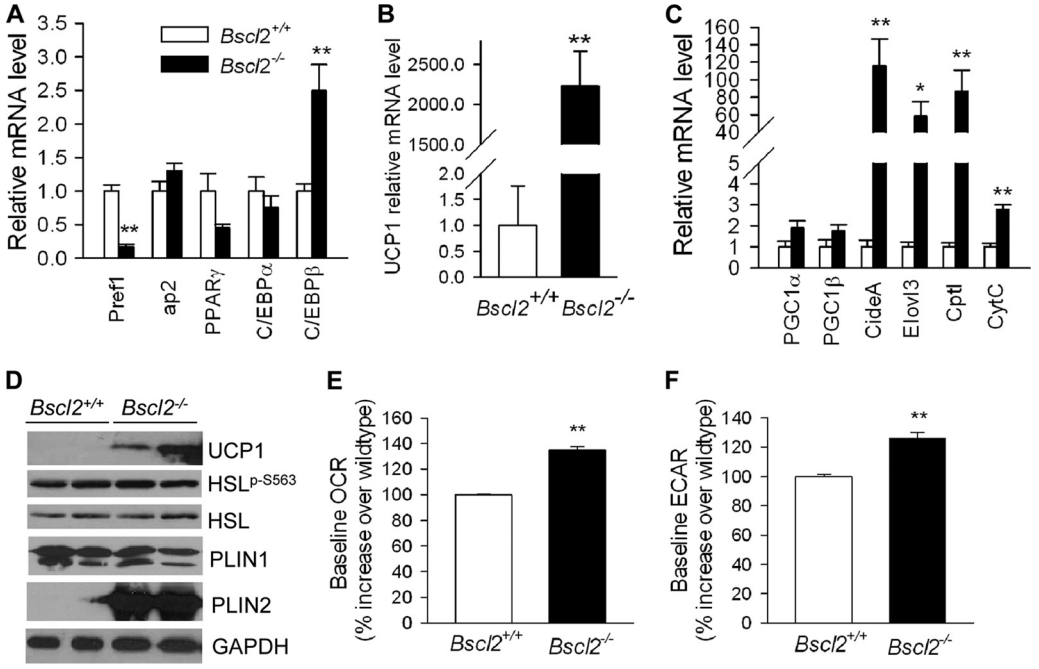

FIG 9 Gene and protein expression in EWAT of wild-type and *Bscl2*$^{-/-}$ mice *in vivo*. (A to C) qPCR analyses of genes involved in adipocyte differentiation (A), UCP1 (B), and brown adipose tissue-specific marker genes (C) in EWAT of 13-week-old nonfasting male wild-type and *Bscl2*$^{-/-}$ mice ($n = 6$). Data were normalized to 3 housekeeping genes (cyclophilin A, Eelf1γ and β-actin genes) based on the Genorm algorithm (http://medgen.ugent.be/genorm/) and are expressed as fold changes relative to wild-type controls. (D) Western blot analyses of lysates extracted from EWAT of 6-week-old male wild-type and *Bscl2*$^{-/-}$ mice. Identical amounts of protein were loaded. GAPDH was used as a loading control. (E and F) Baseline OCR (E) and ECAR (F) in day 4 differentiating *Bscl2*$^{+/+}$ and *Bscl2*$^{-/-}$ MEFs. The basal rates shown represent averages of 10 time points each with 4 wells and are presented as percent increases over wild-type baseline values. *, $P < 0.05$; **, $P < 0.005$ (between the two genotypes).

lymphoblastoid cell lines derived from CGL2 patients (6). At later stages of differentiation, supersized LDs make their appearance (Fig. 3D), a phenotype that was also observed in yeast Fld1/Bscl2 mutants (15, 41). These supersized LDs may represent a compensatory response of the cells in an attempt to minimize the total surface area of the LDs to limit lipolysis as the size of LDs has been found to be inversely correlated with the rate of lipolysis (29, 32).

It is noteworthy that PLIN2 mRNA is highly elevated in the beginning of adipocyte differentiation and that its level remains constant throughout the differentiation. However, PLIN2 protein is degraded by proteasome degradation pathways and has been shown to be absent from mature adipocytes once PLIN1 makes its presence (7). We noted the predominant upregulation of PAT family LDP PLIN2 both *in vitro* in the differentiating *Bscl2*$^{-/-}$ cells and *in vivo* in the EWAT of *Bscl2*$^{-/-}$ mice. A similar phenomenon has also been observed in mice with Fsp27 and PLIN1 ablation, which exhibited elevated lipolysis (32, 40). More importantly, PLIN2 protein expression was previously shown to reappear as a response to protect lipid droplets from lipolysis when PLIN1 is chronically hyperphosphorylated by hormone-induced lipolysis (16), a finding that corroborates our observation in differentiating *Bscl2*$^{-/-}$ cells and EWAT that exhibit unbridled cAMP/PKA-mediated lipolysis. Collectively, these findings show that the rampant stimulated lipolysis leads to the aborted adipose differentiation, resulting in the presence of residual much smaller and immature adipocytes that express a massive amount of Plin2 both *in vitro* and *in vivo*. The dynamic LD changes and adipocyte turnover during adipogenesis of Bscl2-deficient cells *in vitro* are substantially different from what has been reported from studies of cultured adipogenic cell lines with Bscl2 knockdown (11, 33), possibly due to the presence of a low but significant level of functional Bscl2 expression in knockdown cells.

Lipolysis-mediated impaired adipocyte differentiation also underlies the congenital generalized loss of adipose tissue in *Bscl2*$^{-/-}$ mice *in vivo*. The residual EWAT of *Bscl2*$^{-/-}$ mice demonstrates higher basal lipolysis. The striking upregulation of UCP1 expression in EWAT of *Bscl2*$^{-/-}$ mice implies the presence of increased cAMP signaling, as cAMP-mediated PKA activation has been demonstrated to be the major pathway that integrates with PPARγ and PGC1α to regulate UCP1 expression in the white adipose tissue depots (36, 46). We could not detect a significant increase in PKA-mediated HSL phosphorylation in the EWAT of adult *Bscl2*$^{-/-}$ mice (Fig. 9D) such as we have demonstrated in differentiating *Bscl2*$^{-/-}$ MEFs (Fig. 6A) and SVCs *in vitro* (see Fig. S5E in the supplemental material). This might be due to the fact that the residual EWAT of adult *Bscl2*$^{-/-}$ mice had reached a late stage of white adipose tissue development very different from that of actively differentiating *Bscl2*$^{-/-}$ cells studied *in vitro*. The EWAT appears to contain altered cell populations, including macrophages which have been shown to infiltrate lipodystrophic adipose tissues (18). Interestingly, the marked upregulation of PLIN2 protein expression in the residual EWAT of *Bscl2*$^{-/-}$ mice (as occurs in *in vitro* differentiating *Bscl2*$^{-/-}$ cells) is readily evident and is reminiscent of the consequences of unbridled lipolysis. Meanwhile, although the residual adipose depots of *Bscl2*$^{-/-}$ mice express a similar level of mature adipocyte markers, the much lower level of Pref1, a preadipocyte marker and an inhibitor of adipocyte differentiation (39), along with the increased C/EBPβ, a

transcription factor required for an early stage of adipogenesis (44), together suggest an enhanced conversion of *Bscl2*$^{-/-}$ preadipocytes to adipocytes *in vivo* to compensate for a marked deficiency of adipocytes resulting from defective terminal adipocyte differentiation in these mice.

Our data show Bscl2 to be an early physiological regulator of cAMP/PKA-stimulated lipolysis whose disruption has a profound effect on adipocyte differentiation. The late differentiation defect can be reversed by a PKA inhibitor (Fig. 6) or a downstream lipase inhibitor (Fig. 5), further underscoring the important role of well-controlled cAMP/PKA-mediated lipolysis in sustaining normal adipogenesis. Ablation of genes such as the PLIN1 and Fsp27 genes results in higher basal lipolysis in mature adipocytes but has no apparent effect on adipocyte differentiation (28, 32), suggesting that cAMP/PKA-stimulated lipolysis, but not basal lipolysis, may play a direct role in adipocyte differentiation. Consequently, the fat loss in *Bscl2*$^{-/-}$ mice is substantially more severe than that observed in the other models. In addition, forced hyperactivation of PPARγ by pioglitazone treatment ameliorates the differentiation defect in *Bscl2*$^{-/-}$ MEFs to only a very minor extent (Fig. 5). Only when the unbridled lipolysis is suppressed by a lipase inhibitor is the differentiation defect reversed with restoration of normal adipocyte differentiation (Fig. 5). These data argue against PPARγ being a downstream target or mediator of Bscl2 action.

It is unclear how an ER BSCL2 protein modulates cAMP signaling pathway. Bscl2 was originally identified as a divergently transcribed gene adjacent to the G protein γ 3 subunit (Gng3) gene (14), whose gene product is involved in G protein-coupled receptor (GPCR) signaling. However, the activation of cAMP/PKA signaling in the absence of Bscl2 was unlikely to have been mediated at the level of β-adrenergic receptors (β-AR), because we found that neither pan-β-AR antagonists [(*S*)-(−)-propranolol hydrochloride] nor the antagonist against the most abundant β3-AR (SR59230A) blocks lipolysis or rescues adipocyte differentiation in *Bscl2*$^{-/-}$ MEFs (data not shown). We note that Bscl2 was found to regulate phospholipid metabolism (6, 15), which could potentially generate downstream lipid mediators that modulate cAMP signaling. The exact pathway whereby Bscl2 controls lipolysis must await further elucidation. A detailed analysis is hampered by the lack of a specific antibody that recognizes the endogenous protein and the fact that transgene-induced expression of Bscl2 in cells *in vitro* generally leads to aggregate formation (11, 26).

There is a complex relationship between cAMP/PKA signaling and the expression of adipose-specific transcription factors and adipose differentiation. Activation of cAMP/PKA and subsequent phosphorylation of cAMP response element binding protein (CREB) is required for upregulation of C/EBPβ and initiation of adipocyte differentiation in 3T3-L1 cells (35, 49). In contrast, chronic activation of cAMP/PKA, through either adrenergic signaling or forskolin, negatively regulates adipose tissue-specific transcription factors such as C/EBPβ, C/EBPα, and/or PPARγ2, impeding adipogenesis in MEFs (Fig. 7) and other different cell types (20, 22, 23, 34). Here we show that in differentiating *Bscl2*$^{-/-}$ cells, the abnormal activation of the cAMP/PKA pathway triggers a marked reduction of adipose-specific transcription factors and their downstream targets and products, leading to the formation of rounded cells that have completely lost their adipocyte phenotype, containing no LDs or adipocyte marker proteins, a process that can be reversed with lipase inhibitors but not PPARγ activation.

In summary, by creating and investigating the mouse genetic equivalent of human CGL2, we have identified Bscl2 as a cell-autonomous determinant of cAMP/PKA-stimulated lipolysis, a process which must be tightly regulated for complete differentiation and maintenance of adipocytes.

ACKNOWLEDGMENTS

The work was supported by grant HL-51586 (to L.C.) and grant P30DK079638 for a Diabetes and Endocrinology Research Center from the U.S. National Institutes of Health. W.C. was supported by a postdoctoral fellowship and a beginning grant-in-aid from the American Heart Association South Central Affiliate (0825134F and 10BGIA3180009, respectively). Fluorescence microscopy resources were supported by grants SCCPR U54 HD-007495 (to B. W. O'Malley), P30 DK-56338 (to M. K. Estes), and P30 CA-125123 (to C. K. Osborne) and by the Dan L. Duncan Cancer Center of Baylor College of Medicine.

We thank members of the Lawrence Chan laboratory for helpful discussions. We also thank Robia Pautler and Lingyun Hu for excellent technical advice.

We have declared that no conflict of interest exists.

REFERENCES

1. **Agarwal AK, Barnes RI, Garg A.** 2004. Genetic basis of congenital generalized lipodystrophy. Int. J. Obes. Relat. Metab. Disord. **28**:336–339.
2. **Agarwal AK, Garg A.** 2003. Congenital generalized lipodystrophy: significance of triglyceride biosynthetic pathways. Trends Endocrinol. Metab. **14**:214–221.
3. **Agarwal AK, et al.** 2003. Phenotypic and genetic heterogeneity in congenital generalized lipodystrophy. J. Clin. Endocrinol. Metab. **88**:4840–4847.
4. **Berardinelli W.** 1954. An undiagnosed endocrinometabolic syndrome: report of 2 cases. J. Clin. Endocrinol. Metab. **14**:193–204.
5. **Bligh EG, Dyer WJ.** 1959. A rapid method of total lipid extraction and purification. Can. J. Biochem. Physiol. **37**:911–917.
6. **Boutet E, et al.** 2009. Seipin deficiency alters fatty acid Delta9 desaturation and lipid droplet formation in Berardinelli-Seip congenital lipodystrophy. Biochimie **91**:796–803.
7. **Brasaemle DL, et al.** 1997. Adipose differentiation-related protein is an ubiquitously expressed lipid storage droplet-associated protein. J. Lipid Res. **38**:2249–2263.
8. **Brasaemle DL, Levin DM, Adler-Wailes DC, Londos C.** 2000. The lipolytic stimulation of 3T3-L1 adipocytes promotes the translocation of hormone-sensitive lipase to the surfaces of lipid storage droplets. Biochim. Biophys. Acta **1483**:251–262.
9. **Brasaemle DL, et al.** 2000. Perilipin A increases triacylglycerol storage by decreasing the rate of triacylglycerol hydrolysis. J. Biol. Chem. **275**:38486–38493.
10. **Brasaemle DL, Wolins NE.** 2006. Isolation of lipid droplets from cells by density gradient centrifugation. Curr. Protoc. Cell Biol. 3.15.1–3.15.12. doi:10.1002/0471143030.cb0315s29.
11. **Chen W, et al.** 2009. The human lipodystrophy gene product Berardinelli-Seip congenital lipodystrophy 2/seipin plays a key role in adipocyte differentiation. Endocrinology **150**:4552–4561.
12. **Cortés VA, et al.** 2009. Molecular mechanisms of hepatic steatosis and insulin resistance in the AGPAT2-deficient mouse model of congenital generalized lipodystrophy. Cell Metab. **9**:165–176.
13. **Cui X, et al.** 2011. Seipin ablation in mice results in severe generalized lipodystrophy. Hum. Mol. Genet. **20**:3022–3030.
14. **Downes GB, Copeland NG, Jenkins NA, Gautam N.** 1998. Structure and mapping of the G protein gamma3 subunit gene and a divergently transcribed novel gene, gng3lg. Genomics **53**:220–230.
15. **Fei W, et al.** 2008. Fld1p, a functional homologue of human seipin, regulates the size of lipid droplets in yeast. J. Cell Biol. **180**:473–482.
16. **Gross DN, et al.** 2006. Dynamics of lipid droplet-associated proteins during hormonally stimulated lipolysis in engineered adipocytes: stabilization and lipid droplet binding of adipocyte differentiation-related protein/adipophilin. Mol. Endocrinol. **20**:459–466.

17. **Haemmerle G, et al.** 2006. Defective lipolysis and altered energy metabolism in mice lacking adipose triglyceride lipase. Science **312**:734–737.
18. **Herrero L, Nayer SHA, Lee J, Shoelson SE.** 2010. Inflammation and adipose tissue macrophages in lipodystrophic mice. Proc. Natl. Acad. Sci. U. S. A. **107**:240–245.
19. **Jimenez MA, Akerblad P, Sigvardsson M, Rosen ED.** 2007. Critical role for Ebf1 and Ebf2 in the adipogenic transcriptional cascade. Mol. Cell. Biol. **27**:743–757.
20. **Klaus S, Seivert A, Boeuf S.** 2001. Effect of the beta(3)-adrenergic agonist CL 316243 on functional differentiation of white and brown adipocytes in primary cell culture. Biochim. Biophys. Acta **1539**:85–92.
21. **Lagouge M, et al.** 2006. Resveratrol improves mitochondrial function and protects against metabolic disease by activating SIRT1 and PGC-1alpha. Cell **127**:1109–1122.
22. **Li H, Fong C, Chen Y, Cai G, Yang M.** 2010. Beta-adrenergic signals regulate adipogenesis of mouse mesenchymal stem cells via cAMP/PKA pathway. Mol. Cell Endocrinol. **323**:201–207.
23. **Lindgren EM, et al.** 2004. Noradrenaline represses PPAR (peroxisome-proliferator-activated receptor) gamma2 gene expression in brown adipocytes: intracellular signalling and effects on PPARgamma2 and PPARgamma1 protein levels. Biochem. J. **382**:597–606.
24. **Liu P, Bartz R, Zehmer JK, Ying Y, Anderson RG.** 2008. Rab-regulated membrane traffic between adiposomes and multiple endomembrane systems. Methods Enzymol. **439**:327–337.
25. **Londos C, et al.** 1999. On the control of lipolysis in adipocytes. Ann. N. Y. Acad. Sci. **892**:155–168.
26. **Magré J, et al.** 2001. Identification of the gene altered in Berardinelli-Seip congenital lipodystrophy on chromosome 11q13. Nat. Genet. **28**:365–370.
27. **Marcinkiewicz A, Gauthier D, Garcia A, Brasaemle DL.** 2006. The phosphorylation of serine 492 of perilipin a directs lipid droplet fragmentation and dispersion. J. Biol. Chem. **281**:11901–11909.
28. **Martinez-Botas J, et al.** 2000. Absence of perilipin results in leanness and reverses obesity in Lepr(db/db) mice. Nat. Genet. **26**:474–479.
29. **Miyoshi H, Perfield JW, II, Obin MS, Greenberg AS.** 2008. Adipose triglyceride lipase regulates basal lipolysis and lipid droplet size in adipocytes. J. Cell Biochem. **105**:1430–1436.
30. **Miyoshi H, Perfield JW, II, et al.** 2007. Control of adipose triglyceride lipase action by serine 517 of perilipin A globally regulates protein kinase A-stimulated lipolysis in adipocytes. J. Biol. Chem. **282**:996–1002.
31. **Miyoshi H, et al.** 2006. Perilipin promotes hormone-sensitive lipase-mediated adipocyte lipolysis via phosphorylation-dependent and -independent mechanisms. J. Biol. Chem. **281**:15837–15844.
32. **Nishino N, et al.** 2008. FSP27 contributes to efficient energy storage in murine white adipocytes by promoting the formation of unilocular lipid droplets. J. Clin. Invest. **118**:2808–2821.
33. **Payne VA, et al.** 2008. The human lipodystrophy gene BSCL2/seipin may be essential for normal adipocyte differentiation. Diabetes **57**:2055–2060.
34. **Rehnmark S, Antonson P, Xanthopoulos KG, Jacobsson A.** 1993. Differential adrenergic regulation of C/EBP alpha and C/EBP beta in brown adipose tissue. FEBS Lett. **318**:235–241.
35. **Reusch JEB, Colton LA, Klemm DJ.** 2000. CREB activation induces adipogenesis in 3T3-L1 cells. Mol. Cell. Biol. **20**:1008–1020.
36. **Robidoux J, et al.** 2005. Selective activation of mitogen-activated protein (MAP) kinase kinase 3 and p38alpha MAP kinase is essential for cyclic AMP-dependent UCP1 expression in adipocytes. Mol. Cell. Biol. **25**:5466–5479.
37. **Seip M, Trygstad O.** 1996. Generalized lipodystrophy, congenital and acquired (lipoatrophy). Acta Paediatr. Suppl. **413**:2–28.
38. **Simha V, Garg A.** 2006. Lipodystrophy: lessons in lipid and energy metabolism. Curr. Opin. Lipidol. **17**:162–169.
39. **Sul HS.** 2009. Pref-1: role in adipogenesis and mesenchymal cell fate. Mol. Endocrinol. **23**:1717–1725.
40. **Sztalryd C, et al.** 2003. Perilipin A is essential for the translocation of hormone-sensitive lipase during lipolytic activation. J. Cell Biol. **161**:1093–1103.
41. **Szymanski KM, et al.** 2007. The lipodystrophy protein seipin is found at endoplasmic reticulum lipid droplet junctions and is important for droplet morphology. Proc. Natl. Acad. Sci. U. S. A. **104**:20890–20895.
42. **Windpassinger C, et al.** 2004. Heterozygous missense mutations in BSCL2 are associated with distal hereditary motor neuropathy and Silver syndrome. Nat. Genet. **36**:271–276.
43. **Wu M, et al.** 2007. Multiparameter metabolic analysis reveals a close link between attenuated mitochondrial bioenergetic function and enhanced glycolysis dependency in human tumor cells. Am. J. Physiol. Cell Physiol. **292**:C125–C136.
44. **Wu Z, Bucher NL, Farmer SR.** 1996. Induction of peroxisome proliferator-activated receptor gamma during the conversion of 3T3 fibroblasts into adipocytes is mediated by C/EBPbeta, C/EBPdelta, and glucocorticoids. Mol. Cell. Biol. **16**:4128–4136.
45. **Xu C, et al.** 2009. Direct effect of glucocorticoids on lipolysis in adipocytes. Mol. Endocrinol. **23**:1161–1170.
46. **Xue B, Coulter A, Rim JS, Koza RA, Kozak LP.** 2005. Transcriptional synergy and the regulation of Ucp1 during brown adipocyte induction in white fat depots. Mol. Cell. Biol. **25**:8311–8322.
47. **Yehuda-Shnaidman E, Buehrer B, Pi J, Kumar N, Collins S.** 2010. Acute stimulation of white adipocyte respiration by PKA-induced lipolysis. Diabetes **59**:2474–2483.
48. **Zechner R, Strauss JG, Haemmerle G, Lass A, Zimmermann R.** 2005. Lipolysis: pathway under construction. Curr. Opin. Lipidol. **16**:333–340.
49. **Zhang JW, Klemm DJ, Vinson C, Lane MD.** 2004. Role of CREB in transcriptional regulation of CCAAT/enhancer-binding protein beta gene during adipogenesis. J. Biol. Chem. **279**:4471–4478.